The Effects of Small Ice Crystals on Cirrus Infrared Radiative Properties

Y. TAKANO AND K. N. LIOU

Department of Meteorology/CARSS, University of Utah, Salt Lake City, Utah

P. MINNIS

Atmospheric Sciences Division, NASA Langley Research Center, Hampton, Virginia

ABSTRACT

Using a model that combines single-scattering properties for spheroidal and hexagonal ice crystals, the thermal infrared radiative properties of cirrus clouds have been investigated. Infrared scattering and absorption properties for randomly oriented spheroids and hexagons are parameterized based on the anomalous diffraction theory and a geometric ray-tracing method, respectively. Using observed ice crystal size distributions, upwelling radiances at the top of cirrus cloudy atmospheres have been computed. Results show that the presence of small ice crystals can produce significant brightness temperature differences between two infrared wavelengths in the 10-μm window. Theoretical results have been compared with observed brightness temperature differences between 8.35 and 11.16 μm and between 11.16 and 12 μm. The observed values were obtained from the High-Spectral Resolution Interferometer Sounder. It is shown that the use of the present nonspherical model for ice crystals in radiative transfer calculations leads to a significantly better interpretation of the observed data than does the use of the spherical model.

1. Introduction

To be successful in the development of satellite retrieval methodologies for the determination of cirrus cloud properties, we must have fundamental scattering and absorption data on the nonspherical ice crystals that are found in cirrus clouds. Recent observations reveal that there may be a large amount of small ice particles, on the order of 10 μm, in cirrus clouds (Platt et al. 1989). Thus, it is important to explore potential differences in the scattering and absorption properties of ice crystals with respect to their sizes and shapes. In this paper, the effects of nonspherical ice crystals on the infrared radiative properties of cirrus clouds are investigated using light scattering and absorption properties of spheroidal and hexagonal particles.

In section 2, we develop efficient parameterization equations for the calculation of the scattering and absorption properties for small ice crystals, based on the anomalous diffraction theory for spheroids. Parameterization formulas are also developed in section 3 for large ice crystals, using results computed from a geometric ray-tracing technique. Section 4 describes applications of the present theoretical analyses to the AVHRR (Advanced Very High Resolution Radiometer) channels and HIS (High-Spectral Resolution Interferometer Sounder) measurements. A summary is presented in the final section.

2. Parameterization for small ice crystals

Because of the hexagonal structure, ice crystals of larger size parameters will produce a number of halo patterns, which are important for the computations of the single-scattering properties. However, the scattering properties for ice crystals of smaller size parameters depend largely on the overall shape but not on the subtle differences in particle structure (e.g., see Dungey and Bohren 1992). Thus, as a first approximation, we may use a spheroidal model to represent ice crystals whose size parameters are less than ~30 at which the geometric ray tracing is not applicable. Latimer (1975, 1980) developed four approximations for the computation of the scattering and absorption properties of spheroids. The AD-I method, the simplest parameterization, can be used to calculate only scattering and extinction cross sections, but not the asymmetry factors for spheroids. Furthermore, the AD-I method does not reproduce accurate results for extinction and absorption cross sections. Although the other three methods can be used to compute the asymmetry factor, as well as scattering and extinction cross sections for spheroids, the computation time required is about 100 times more than the AD-I method because of the additional two angular integrations involved. None of these methods

Corresponding author address: Dr. Y. Takano, University of Utah, Department of Meteorology, 809 Wm. C. Browning Building, Salt Lake City, UT 84112.

is suitable for the parameterization of the single-scattering properties involving ice crystals. For this reason, we have developed a procedure to compute the single-scattering parameters, including the asymmetry factor for small ice crystals.

For a spheroid, the equivalent spherical radius may be expressed by

$$a_s = a_e[v/(\cos^2\zeta + v^2 \sin^2\zeta)^{1/2}]^{k_1}, \quad (1)$$

where ζ is the angle between an incident direction and the rotation axis of the spheroid; a_e is the radius of the spheroid, that is, the length of the short (long) semiaxis for prolate (oblate) spheroids; v is the axial ratio; and k_1 is an empirical constant. The extinction or scattering cross section of a spheroid may be expressed by

$$C(\zeta) = Q_{sph}\pi a_e^2[(\cos^2\zeta + v^2 \sin^2\zeta)^{1/2}]^{k_2}, \quad (2)$$

where Q_{sph} is the optical efficiency factor from the Mie theory for a sphere of radius, a_s, and k_2 is an empirical constant. If k_2 is 1 in Eq. (2), the right-hand side becomes Q_{sph} times the geometric shadow area of a spheroid. The extinction or scattering cross section for randomly oriented spheroids is given by

$$\bar{C}_{e,s} = \int_0^{\pi/2} C_{e,s}(\zeta) \sin\zeta d\zeta. \quad (3)$$

The unknown constants, k_1 and k_2, in Eqs. (1) and (2) are determined by matching the extinction efficiency, $\bar{C}_e/\bar{A}$, with that computed by the exact method shown in Fig. 2 of Asano and Sato (1980), where $\bar{A}$ is the average geometric cross section of a spheroid, as follows:

$$\left.\begin{array}{lll} k_1 = 1.0, & k_2 = 0.98, & \text{for} \quad v \geq 1 \\ k_1 = 0.96, & k_2 = 1.08, & \text{for} \quad v < 1 \end{array}\right\}. \quad (4)$$

To determine k_1 and k_2, we have used spheroids whose aspect ratios are 2, 3, and 5, a refractive index of 1.33, and size parameters ranging from 0 to 18. The deviation of k_1 and k_2 from 1 is an improvement with respect to the AD-I method. As shown in Eq. (4), k_1 and k_2 are close to 1 for prolate spheroids ($v \geq 1$) but deviate from 1 for oblate spheroids ($v < 1$). In the latter case, by reducing k_1 to a value less than 1, the effect of nonsphericity on the extinction efficiency factor, which is overestimated by the Latimer method, is suppressed. As a result, the first peak position for the extinction efficiency becomes closer to the exact value. Increasing k_2 to a value larger than 1 would indirectly suppress the surface-wave (ripple) effect, which frequently appears in the case of a sphere via Q_{sph}. Because of this adjustment, the extinction efficiency would not be increased to values overestimated by the AD-I method.

The single-scattering albedo is given by

$$\tilde{\omega} = \frac{\bar{C}_s}{\bar{C}_s + \bar{C}_{a,\text{VES}}}, \quad (5)$$

where $C_{a,\text{VES}}$ is the absorption cross section for the volume-equivalent sphere. This parameter has been introduced because the anomalous diffraction theory is not a good approximation for the absorption cross section, as pointed out previously. When the shape of spheroid becomes flat (plate) or elongated (column), scattered light rays are largely confined to forward directions. This effect is equivalent to the condition that the scattering body is more transparent. For this reason, the asymmetry factor may be parameterized for spheroids using spheres by reducing the real refractive index as follows:

$$\frac{m_r^*}{m_r} = \begin{cases} 1 + \sum_{n=1}^{3} a_n(v - 1)^{n+1}, & \text{for} \quad v \geq 1 \\ 1 + \sum_{n=1}^{3} b_n(1/v - 1)^{n+1}, & \text{for} \quad v < 1, \end{cases} \quad (6)$$

where the empirical coefficients are $a_1 = -0.01073$, $a_2 = -0.001293$, $a_3 = 0.000744$, $b_1 = 0.003289$, $b_2 = -0.01339$, and $b_3 = 0.002585$. The procedure for determining these coefficients is described below.

In order to improve the approximation, we also adjust the particle size for spheres in the form

$$\frac{a_s^*}{a_s} = \begin{cases} 1 + \sum_{n=1}^{3} c_n(v - 1)^{n+1}, & \text{for} \quad v \geq 1 \\ 1 + \sum_{n=1}^{3} d_n(1/v - 1)^{n+1}, & \text{for} \quad v < 1, \end{cases} \quad (7)$$

where the empirical coefficients are $c_1 = 0.06188$, $c_2 = -0.02531$, $c_3 = 0.003438$, $d_1 = 0.0275$, $d_2 = -0.00875$, and $d_3 = 0.00125$. The averaged asymmetry factor with respect to orientation can be obtained from

$$\bar{g} = \frac{\int_0^{\pi/2} g_{sph}(m_r^*, a_s^*)C_s(\zeta, m, a_s) \sin\zeta d\zeta}{\int_0^{\pi/2} C_s(\zeta, m, a_s) \sin\zeta d\zeta}, \quad (8)$$

where g_{sph} is the asymmetry factor computed from the Mie theory for a sphere of radius, a_s^*, and for the complex refractive index, $m_r^* - im_i$. In order to obtain the coefficients in Eqs. (6) and (7), we first assume a certain value of v. Subsequently, $\bar{g}$ is calculated from Eq. (8) against several values of m_r^* and a_s^*. To get the best fit with respect to the exact asymmetry factor for spheroids shown in Fig. 5 of Asano and Sato (1980), m_r^* and a_s^* are determined for each value of v. Under the condition that $m_r^* = m_r$ and $a_s^* = a_s$, $v = 1$. The

ratios, m_i^*/m_r and a_s^*/a_s, are then fitted numerically in terms of polynomials of $v-1$ or $1/v-1$. We find that a third-order polynomial expansion is sufficient to achieve an accuracy within 1%.

Figure 1 shows the extinction efficiency, asymmetry factor, and single-scattering albedo for randomly oriented spheroids with an axial ratio of 2 as a function of the area-equivalent size parameter, $x_g = 2\pi r_g/\lambda$, where r_g is the radius of the area-equivalent sphere. The area-equivalent spheres are used because they will produce about the same optical depth as randomly oriented nonspherical particles. The crosses and circles are computed from the exact method, whereas the dashed and solid lines are computed from the parameterized equations for the wavelengths of 11 and 12 μm. The accuracy of the parameterization for small ice crystals is within about 1%, which is reasonably accurate. As shown in this figure, the absorption efficiencies for ice crystals for these two wavelengths can differ by as much as a factor of 2. This difference could provide a means for the detection of small ice crystals using the radiances measured with radiometers aboard satellites (e.g., Prabhakara et al. 1988).

3. Parameterization for large ice crystals

For larger size parameters, the hexagonal ice crystal model is used to develop parameterization equations for scattering and absorption properties of ice crystals. Parameterization of the single-scattering albedo may be performed using the results computed from a geometric ray-tracing technique for hexagonal crystals (Takano and Liou 1989a; Liou et al. 1990). Based on numerical calculations involving a number of wavelengths, crystal lengths, D, and crystal widths, w, the single-scattering albedo can be expressed in the form

$$\tilde{\omega} = \begin{cases} 1 - \displaystyle\sum_{n=1}^{4} f_n z^n, & \text{for} \quad z < 0.4 \quad (9a) \\[2mm] 1 - 0.47[1 - \exp(-1.5051 z^{0.6789})], \\[1mm] \qquad\qquad\qquad\qquad \text{for} \quad z \geqslant 0.4, \quad (9b) \end{cases}$$

where z is a physical parameter, defined by

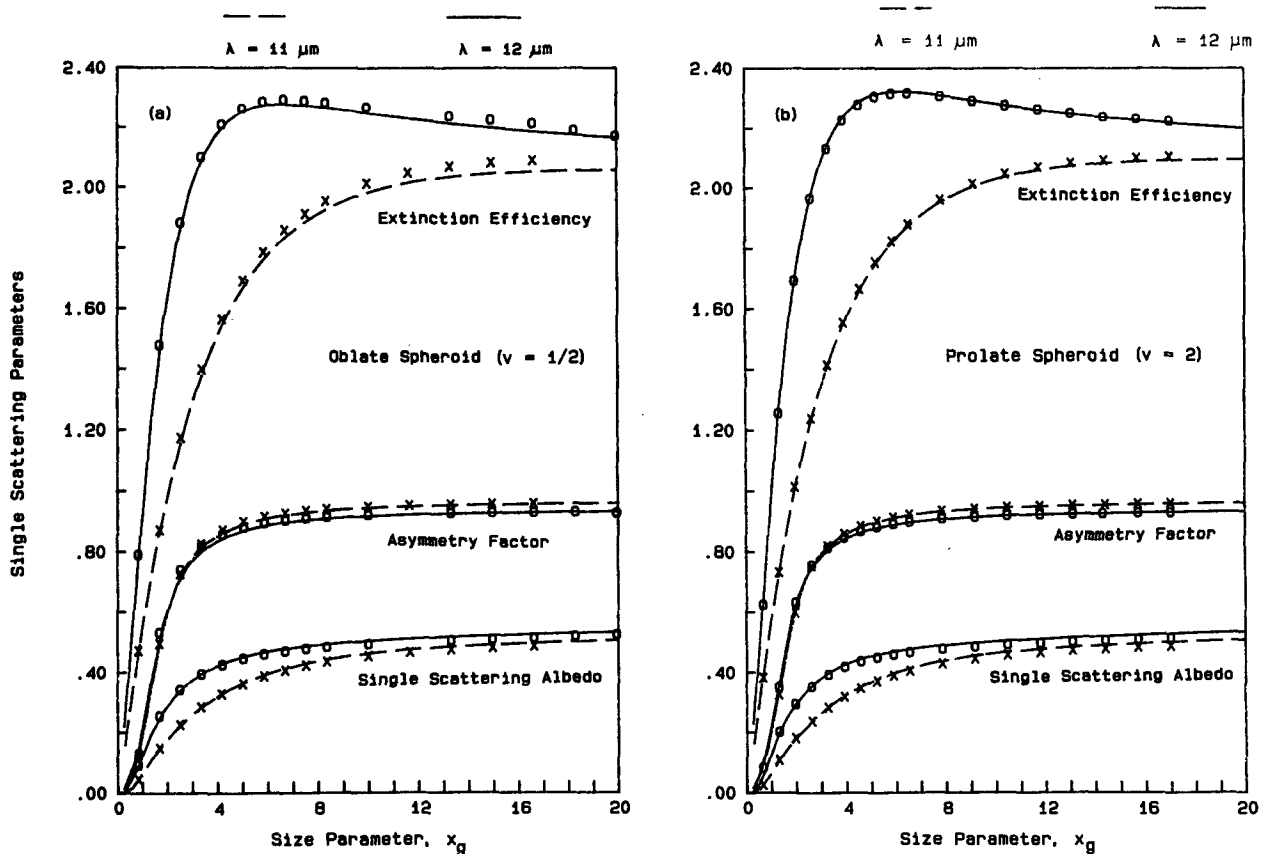$$z = \frac{4\pi m_i}{\lambda} \frac{w}{2} \frac{3\sqrt{3}(D/w)}{\sqrt{3}+(D/w)}, \quad (10)$$

FIG. 1. Comparison of the single-scattering properties for randomly oriented small (a) oblate and (b) prolate spheroids computed from parameterization (solid and dashed lines) and the exact method (circles and crosses). The complex refractive indexes of ice used are $m = 1.0925 - 0.2480i$ at $\lambda = 11$ μm and $m = 1.280 - 0.4133i$ at $\lambda = 12$ μm.

and the numerator and denominator in the last term of this equation are proportional to the volume and cross sectional area of an ice crystal, respectively. The coefficients in Eq. (9) are as follows: $f_1 = 1.1128$, $f_2 = -2.5576$, $f_3 = 5.6257$, and $f_4 = -5.9498$. These functional forms were adopted for the following reason. When z is small, $1 - \tilde{\omega}$ is proportional to z. As a result, $1 - \tilde{\omega}$ may be expressed in terms of a polynomial function in z for weakly absorbing cases. For large z, on the other hand, the single-scattering albedo, $\tilde{\omega}$, approaches a constant value. Thus, it may be expressed by an exponential function for cases involving intense absorption. The parameterized equations [Eqs. (9a) and (9b)] give an accuracy of better than 1% and 3% for small and large values of z, respectively.

As shown in Fig. 1, the asymmetry factors for large-size parameters are nearly constant because of significant absorption. In view of this pattern, the asymmetry factor for spheroids may be used with size parameters of $x_g = 50$ calculated from Eq. (8) as a replacement for the asymmetry factor for large crystals with size parameters larger than 30.

The extinction efficiency may be parameterized in the form

$$Q_e(x) = 2 + \frac{x_c}{x}[Q_e(x_c) - 2],\qquad (11)$$

where $Q_e = 2$ when $x \to \infty$, and $Q_e = Q_e(x_c)$ at the crossover point, x_c. This functional form was developed in view of the fact that the extinction efficiency approaches monotonically to 2 when the size parameter becomes large for absorbing wavelengths. The crossover point is the size parameter, which demarcates the parameterizations for small and large ice crystals. We shall discuss the manner in which this point is determined. Figures 2a and 2b show the composite single-scattering albedo for randomly oriented flat and elongated particles with an axial ratio of 2 as a function of the size parameter, x_g. The solid lines are calculated from the parameterization for large crystals [Eq. (9)], whereas the dashed lines are calculated from the parameterization for small crystals [Eq. (5)]. For comparison, the values computed by the exact method are represented by circles. From these figures, the crossover point for the single-scattering albedo is determined to be about 20 in units of the area-equivalent size parameter. For the extinction efficiency, we find a value of 30 for the crossover point.

4. Application to satellite remote sensing

Using the preceding parameterizations, we have computed the scattering and absorption properties for a number of ice crystal size distributions. The effects of small ice crystals on the infrared radiative properties of cirrus clouds are investigated using the adding method for radiative transfer (Takano and Liou 1989b;
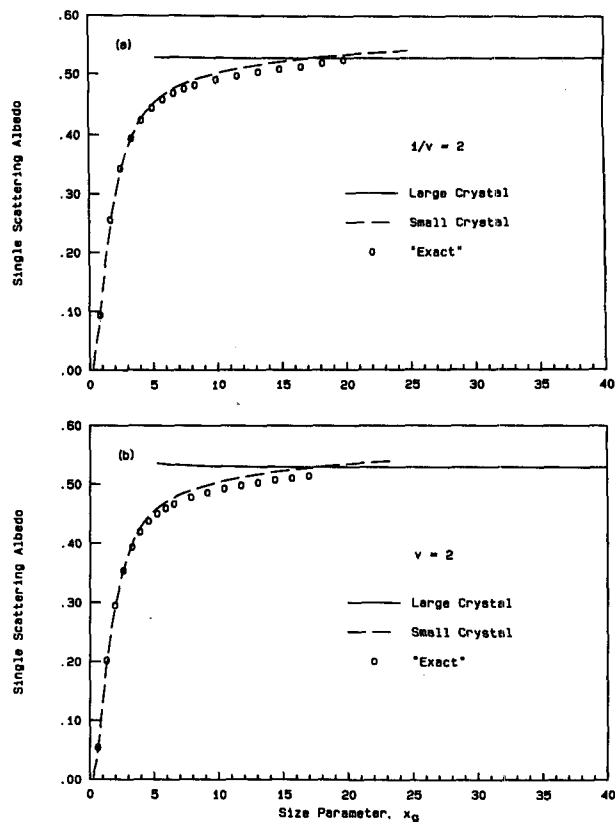

FIG. 2. Single-scattering albedo for randomly oriented (a) flat and (b) elongated particles with an axial ratio of 2 at a wavelength of 12 μm computed from parameterizations for large crystals (solid line) and small crystals (dashed line) and from the exact method (circles).

Liou et al. 1990). In the computation of infrared radiative transfer, we have used the Henyey–Greenstein phase function in terms of the asymmetry factor parameterization described in sections 2 and 3.

In Fig. 3, the computed brightness temperature difference (BTD) between 11 and 12 μm involving cirrus cloud condition is plotted against the computed brightness temperature at the 11-μm wavelength. In this computation, randomly oriented prolate spheroids and hexagonal crystals with an axial ratio of 3 are used to represent columnar ice crystals. Hereafter, this model is called "spheroid/hexagon" for simplicity. For the purpose of comparison, the area-equivalent sphere is also used to approximate the shape of ice crystals. As pointed out earlier, the area-equivalent spheres will produce about the same optical depth as randomly oriented ice crystals if the number densities of the two remain the same. Two model ice crystal size distributions are adopted in this figure (Takano and Liou 1989a). The model cirrus uncinus represents a typical size distribution for cirrus clouds containing larger ice crystals, whereas the model cold cirrus (the term cold is used here for the classification of ice crystal size dis-
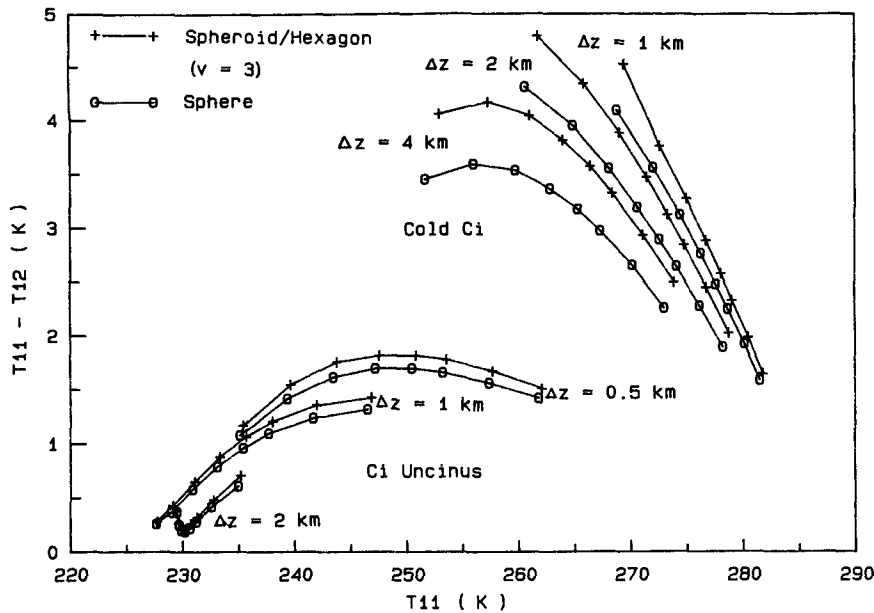
FIG. 3. Computed brightness temperature difference (BTD) between wavelengths of 11 and 12 μm versus computed brightness temperature at the 11-μm wavelength in a cirrus cloud condition. For a given cloud thickness, Δz, each line corresponds to eight computed values associated with eight viewing nadir angles.

tribution) represents a typical particle size distribution for cirrus clouds consisting of small ice crystals. The temperature and humidity profiles used in the calculations correspond to the *U.S. Standard Atmosphere*. The cirrus cloud temperature is assumed to be 226 K in both models. This temperature corresponds to an altitude of ~9 km. In the case of cirrus uncinus, the BTD and the effect of nonsphericity of cloud particles on the brightness temperature are small. However, in the case of cold cirrus, the BTD is noticeable and the effect of nonsphericity of cloud particles on the brightness temperature becomes significant.

Figure 4 is a scatter diagram of the BTD consisting of several hundred points collected for about four hours under cirrus cloud conditions (Ackerman and Smith 1990; and Ackerman et al. 1990). The data were obtained by the HIS aboard the *NASA ER-2* during the period of FIRE. The envelopes are results computed from the present theoretical model. The solid envelope is drawn to cover two sets of theoretical values using randomly oriented "spheroids/hexagons" with axial ratios of 3 and 5. The dashed envelope corresponds to the case involving area-equivalent spheres. These envelopes are derived from a large set of data points computed by varying the cloud thickness, size distribution (including small ice crystals less than 20 μm by extrapolation), and surface temperature. As shown in Fig. 3, large BTDs are related to small crystals. For larger temperature differences, the dashed envelope (spheres) significantly deviates from the observed data.

However, the solid envelope (spheroids/hexagons) covers the observed data corresponding to the main part of cirrus clouds. If the lines connecting the origin and the centers of the envelope are used for error anal-
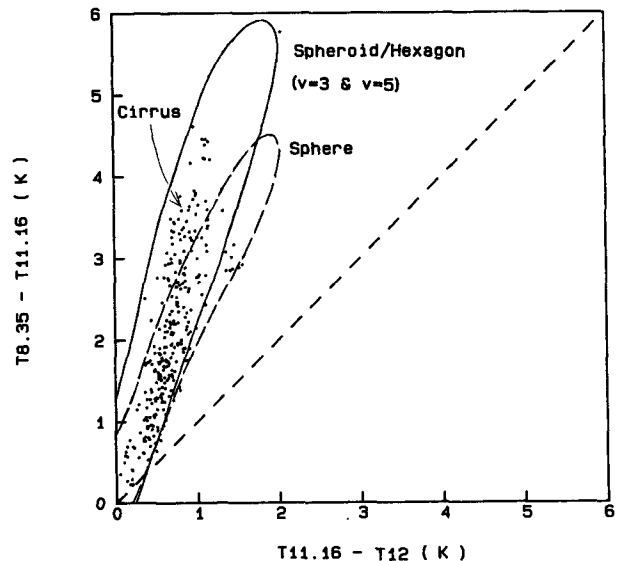

FIG. 4. Scatter diagram of brightness temperature difference (BTD) between 8.35 and 11.16 μm versus BTD between 11.16 and 12 μm observed with the HIS at the nadir direction. Two computed envelopes involving the spheroid/hexagon and sphere models are shown for interpretation.

yses, the root-mean-square errors for the spheroid/hexagon and sphere models are 0.237 and 0.381 K, respectively. These comparisons illustrate that the data observed from the HIS can be more reliably interpreted by taking into account the nonsphericity of small ice crystals. The difference between the spheroid/hexagon and sphere models in this figure can be explained from the single-scattering property of ice crystals, which is described below.

As shown in Table 1, the differences in the single-scattering properties between the wavelengths of 12 and 11.16 μm do not significantly depend on the particle shape due to large absorption of ice at these wavelengths. As a result, $(T_{11.16} - T_{12})$ in Fig. 4 shows little difference between the two models. However, at λ = 8.35 μm, there are noticeable differences between the two models in the single-scattering albedo, $\tilde{\omega}$, and the asymmetry factor, g, due to relatively weak absorption of ice at this wavelength (m = 1.2985 − 0.03724i). The single-scattering albedo for the spheroid/hexagon model is larger than that for the sphere model. This is due to the fact that the volume of the area-equivalent spheres is greater than that of spheroids/hexagons. Also, the asymmetry factor for the spheroids/hexagons is greater than that for the spheres (see Fig. 5 of Asano and Sato 1980). For this reason, $T_{8.35}$ for the nonspherical model is larger than $T_{8.35}$ for the spherical model. In the case of a spheroid/hexagon model, radiation emitted from the surface with higher temperatures is scattered by cloud particles to more forward directions. If the volume-equivalent sphere is used, the radius is smaller than that of the area-equivalent sphere. It follows that the computed envelope for spheres depicted in Fig. 4 would deviate farther from

the observed points corresponding to cirrus clouds. Thus, even if the volume-equivalent sphere is employed, it would not successfully interpret the observed data.

In addition, at λ = 11.16 and 12 μm, the asymmetry factor for spheroids/hexagons is slightly smaller than that for spheres, as shown in Table 1. This feature, which differs from the aforementioned feature associated with the 8.35-μm wavelength, can be explained as follows: At λ = 11.16 and 12 μm, the scattered energy is largely contributed from diffraction and external reflection due to intensive absorption. The intensity distribution associated with externally reflected light for randomly oriented nonspherical particles is the same as that for the area-equivalent spheres. Thus, the difference in the asymmetry factor results from the difference in the diffracted component. As shown in Fig. 7 of Takano and Asano (1983), the diffracted light for spheres is confined to more forward directions than for spheroids. For this reason, the asymmetry factor for spheroids is slightly smaller than that for spheres at these wavelengths.

5. Summary

The effects of small ice crystals on the infrared radiative properties of cirrus clouds have been evaluated using the spheroidal and hexagonal particle model. For small-size parameters, the Mie solutions are adjusted to match with the exact spheroidal solution using the anomalous diffraction theory. For large-size parameters, the single-scattering properties for hexagonal particles are computed from a geometric ray-tracing technique and parameterized using known mathematical equations. With these parameterizations, the scattering and absorption properties for typical ice crystal size distributions (cold cirrus, cirrus uncinus, and so on) are calculated. Subsequently, the infrared radiative properties of cirrus clouds are computed from the adding method for radiative transfer. Small ice crystals produce substantial differences in temperature between two infrared wavelengths. The BTDs observed by the HIS during the period of FIRE are in better agreement with the values computed from the spheroid/hexagon model than those from the sphere model. Nonsphericity of ice crystals must be accounted for in the interpretation of radiances/brightness temperatures observed from space under cirrus cloudy conditions.

TABLE 1. Single-scattering parameters for the size distribution involving cold cirrus at three wavelengths. β_e is the extinction coefficient, $\tilde{\omega}$ is the single-scattering albedo, and g is the asymmetry factor. The range of the particle size is from 20 to 750 μm for the average.

λ (μm)	β_e (km^{-1})	$\tilde{\omega}$	g
Prolate spheroid/hexagon (v = 5)			
12.00	0.1831	0.5043	0.8843
11.16	0.1507	0.4470	0.9087
8.35	0.2232	0.7780	0.9235
Prolate spheroid/hexagon (v = 3)			
12.00	0.1888	0.4911	0.8923
11.16	0.1613	0.4485	0.9167
8.35	0.2365	0.7499	0.9165
Area-equivalent sphere			
12.00	0.1933	0.4701	0.9046
11.16	0.1727	0.4437	0.9296
8.35	0.2248	0.6788	0.8883

REFERENCES

Ackerman, S. A., and W. L. Smith, 1990: Inferring cloud microphysical properties from high resolution spectral measurements in the 8–13-μm window region. Preprints, *Seventh Conf. on Atmospheric Radiation,* San Francisco, Amer. Meteor. Soc., 6–8.

——, ——, J. D. Spinhirne, and H. E. Revercomb, 1990: The 27–28 October 1986 FIRE IFO cirrus case study: Spectral properties of cirrus clouds in the 8–12-μm window. *Mon. Wea. Rev.,* **118,** 2377–2388.

Asano, S., and M. Sato, 1980: Light scattering by randomly oriented spheroidal particles. *Appl. Opt.,* **19,** 962–974.

Dungey, C. E., and C. F. Bohren, 1992: Backscattering by nonspherical hyrometeors as calculated by the coupled-dipole method: An application in radar meteorology. *J. Atmos. Oceanic Technol.,* submitted.

Latimer, P., 1975: Light scattering by ellipsoids. *J. Colloid Interface Sci.,* **53,** 102–109.

——, 1980: Predicted scattering by spheroids: Comparison of approximate and exact methods. *Appl. Opt.,* **19,** 3039–3041.

Liou, K. N., Y. Takano, S. C. Ou, A. J. Heymsfield, and W. Kreiss, 1990: Infrared transmission through cirrus clouds: A radiative model for target detection. *Appl. Opt.,* **29,** 1886–1896.

Platt, C. M. R., J. D. Spinhirne, and W. D. Hart, 1989: Optical and microphysical properties of a cold cirrus cloud: Evidence for regions of small ice particles. *J. Geophys. Res.,* **94,** 11 151–11 164.

Prabhakara, C., R. S. Fraser, G. Dalu, M. C. Wu, and R. J. Curran, 1988: Thin cirrus clouds: Seasonal distribution over oceans deduced from *Nimbus-4* IRIS. *J. Appl. Meteor.,* **27,** 379–399.

Takano, Y., and S. Asano, 1983: Fraunhofer diffraction by ice crystals suspended in the atmosphere. *J. Meteor. Soc. Japan,* **61,** 289–300.

——, and K. N. Liou, 1989a: Solar radiative transfer in cirrus clouds. Part I: Single-scattering and optical properties of hexagonal ice crystals. *J. Atmos. Sci.,* **46,** 3–19.

——, and ——, 1989b: Solar radiative transfer in cirrus clouds. Part II: Theory and computation of multiple scattering in an anisotropic medium. *J. Atmos. Sci.,* **46,** 20–36.